Journal of Fluorescence (2019) 29:1227–1239
https://doi.org/10.1007/s10895-019-02434-9

ORIGINAL ARTICLE

Combustion Synthesis of ZnO/ZnS Nanocomposite Phosphors

Majid Zahiri [1] · Mahdi Shafiee Afarani [1] · Amir Masoud Arabi [2]

Received: 6 April 2019 / Accepted: 3 September 2019 / Published online: 12 October 2019

Abstract

In the present study, combustion synthesis of zinc oxide and zinc sulfide nanoparticles as well as their composite was studied using zinc nitrate and thioacetamide as starting materials, and ethylene glycol as fuel. The influence of different parameters such as oxidizer to fuel (O:F) ratios and calcination process on the structure, microstructure, photoluminescence and optical properties was studied. X-ray diffraction (XRD) patterns showed different combinations of wurtzite structure for zinc oxide and zinc sulfide phases obtained using different O:F ratios of 1:1 and 2:3. Scanning electron microscopy (SEM) micrographs revealed that particles with different morphologies were synthesized depending on the O:F ratio. Besides, nanometer particles, or even quantum dots, could be obtained. Transmission electron microscopy (TEM) micrographs also showed the formation of zinc oxide/ zinc sulfide quantum dots composite using ethylene glycol fuel with O:F ratio of 2:3. Fourier transformed infrared (FTIR) analysis of samples showed carbon bonds of carbonaceous matters in addition to Zn-O and Zn-S bonds due to incomplete combustion. Photoluminescent emission spectra indicated that the highest intensity of emission in blue-green region was obtained from the particle synthesized using ethylene glycol and O:F ratio of 2:3, which may be related to the high density of lattice defects. Band gaps estimated using UV-visible (UV-Vis) spectra were 3.4 and 5.4 eV which can be assigned to the dual nature of particles: in some parts quantum size and in the other parts nanosize particles.

Keywords Solution combustion synthesis · ZnO/ZnS nanocomposite · Photoluminescence properties · Band gap · Oxidizer to fuel ratios

Introduction

Zinc oxide/ zinc sulfide (ZnO/ZnS) nanoparticles are used in different applications including solar cells, optical coatings, photocatalysts, nanosensors, gas sensors, inks for field-effect transistors (FETs), nanopigments, and antibacterial materials in medicine and biology [1–10]. Investigations have shown that ZnS is the most relevant candidate for electroluminescent devices [11]. Zinc oxide and zinc sulfide have been synthesized via different methods including precipitation [12, 13], hydrothermal [14, 15], and combustion [16, 17] methods. The combustion synthesis process is a low cost and high speed process for the production of different ceramic materials [18, 19]. Solution combustion synthesis is relatively a novel combustion method for synthesis of different oxide materials which mostly uses metal nitrates as starting material, as well as urea, glycine, ethylene glycol, etc. as fuel [20–22]. Synthesis begins by solving the starting materials and the fuel in an appropriate solvent, following by heating the solution to evaporate some of the solvent in order to obtain a gel. The process continues by instantaneous combustion of the gel to form the desired product. Nitrate bonds are broken under combustion condition and oxide bonds are formed instead. Providing the process is performed completely, products will have a homogeneous structure [23–24, 25]. Recently, microwaves have been applied to complete the combustion reaction at shorter reaction times. Since a high level of energy is liberated in a short time, the product will be more homogeneous [26,27]. To the best of our knowledge, simultaneous synthesis

✉ Mahdi Shafiee Afarani
shafiee@eng.usb.ac.ir

✉ Amir Masoud Arabi
aarabi@icrc.ac.ir

Majid Zahiri
majidzahiri.1992@yahoo.com

[1] Department of Materials Engineering, Faculty of Engineering, University of Sistan and Baluchestan, Zahedan, Iran

[2] Department of Inorganic Pigments and Glazes, Institute for Color Science and Technology (ICST), Tehran, Iran

of these phases via combustion route is not reported widely, although many efforts have been conducted on the synthesis of ZnS and ZnO nanoparticles.

In our previous study [28], ZnO/ZnS composite powders were synthesized by one-step solution combustion method using thiourea both as the combustion fuel and sulfur source. Results showed that ZnO/ZnS composite particles were highly agglomerated in the micrometer scale.

The aim of the present work was the synthesis of ZnO/ZnS quantum dots by solution combustion method. Effect of oxidizer to fuel (O:F) ratios on the chemical composition, structure, microstructure and photoluminescence properties were investigated.

Experimental

Zinc nitrate hexahydrate (Zn $(NO_3)_2.6H_2O$, MERCK), thioacetamide (C_2H_5NS, MERCK) Ethylene Glycol (EG, $C_2H_6O_2$, MERCK) were used as an oxidizer, sulfur source and a fuel, respectively. All chemical compounds were in chemical grades.

ZnO/ZnS ratios were calculated according to the stoichiometric equations as follows:

$$Zn\ (NO_3)_2.6\ H_2O + C_2H_6O_2 \rightarrow ZnO + N_2 + 9H_2O + 2CO_2 \quad (1)$$

$$CH_3CSNH_2 + H_2O \rightarrow CH_3CONH_2 + H_2S \quad (2)$$

$$Zn(NO_3)_2.6\ H_2O + H_2S + C_2H_6O_2 \rightarrow ZnS + N_2 + 10H_2O + 2CO_2 \quad (3)$$

There was a competition between solution combustion reactions for the formation of ZnO and ZnS in four steps: i) formation of viscous gel of oxidizer (zinc nitrate), sulfur source (thioacetamide) and fuel (ethylene glycol), ii) solution combustion synthesis of ZnO (eq. 1) iii) decomposition of thioacetamide [29] (eq. 2) and iv) solution combustion synthesis of ZnS (eq. 3).

As a typical procedure, stoichiometric ratio (1:1) of oxidizer and fuel, typically 3 g zinc nitrate and 0.62 g Ethylene Glycol fuel were dissolved in 20 mL aqueous solution containing nitric acid to adjust the pH value in the range of 3–4. The solution was stirred at 80–100 °C for 2 h until a yellow gel-like participate was formed. Further heating at 100 °C resulted in the combustion of the obtained participate by the following reaction (Eq.1).

ZnO/ZnS was synthesized by the above-mentioned procedure except adding 0.75 g thioacetamide two-three minutes before the formation of viscose gel. So, the combustion was happened through eq.2 and eq. 3, simultaneously. In some cases, as-synthesized powders were calcined (post heated) at 400–600 °C for 1 h using an electric furnace. The heating rate from room temperature to calcination temperature was set at 20 °C min^{-1}.

Microstructural investigations were performed using scanning electron microscope (SEM, KYKY EM3900) and transmission electron microscope (TEM, Philips CM 120). The mean particle size of the samples was determined using image processing software (Image J 1.44p). X-ray diffraction method (Bruker, Advance D8) was used for structural characterization. Mean crystallite size of the powders was determined using the Scherrer equation ($d_{Scherrer} = 0.9\lambda/\beta\ \cos\ \theta$). Luminescence properties of the synthesized samples were studied by photoluminescence (PL) spectrophotometer (Perkin-Elmer LS55) with the exciting wavelength of 360 nm. Fourier transform infrared spectroscopy (FTIR, Bruker TENSOR II) equipped with platinum ATR accessory with the robust diamond crystal was applied to determine chemical compositions. UV-visible absorption spectra were measured using Perkin Elmer UV–Vis spectrophotometer (Lambda 25). Band gaps were estimated by plotting $(\alpha h\nu)^2$ curves versus $h\nu$ based on the work of J. Tauc and Menth [30], where α is the absorption coefficient, h is the Plank constant and ν is the frequency (s^{-1}).

Results and Discussion

Structural Analysis

Figure 1a, b show XRD patterns of ZnO and ZnO/ZnS particles synthesized using ethylene glycol fuel and different O:F ratios, respectively. As shown, ethylene glycol fuel led to the formation of ZnO (card no. 0704–076-01) in zinc oxide particles (Fig. 1a) and combination of ZnO and Sphalerite ZnS (00–001-0792) in ZnO/ZnS composite powders (Fig. 1b) as dominant phases. Stoichiometric ratio (O:F of 1:1) resulted in crystallinity of powders with narrower peaks. However, increasing the O:F ratio from 1:1 to 2:3 causes incomplete reaction and, consequently, lower crystallinity of the particles.

The effect of combustion on the structure in the presence of rich ethylene glycol fuel (O:F equal to 2:3) and different thioacetamide to nitrate (T:N) ratios is shown in Fig. 2. As illustrated, pure ZnS phase with higher intensity peaks was obtained by increasing the amount of thioacetamide. It is because of more availability of sulfur source due to more decomposition of thioacetamide. Broadening of the peaks in T:N of 2 and 2.5 can be related to the formation of nanocrystallites.

Primary results revealed that the samples synthesized with ethylene glycol had some darkness due to incomplete fuel combustion and showed no luminescence emission under UV cabinet. So, they were calcined at 600 °C just for 3 min to suppress crystallite growth.

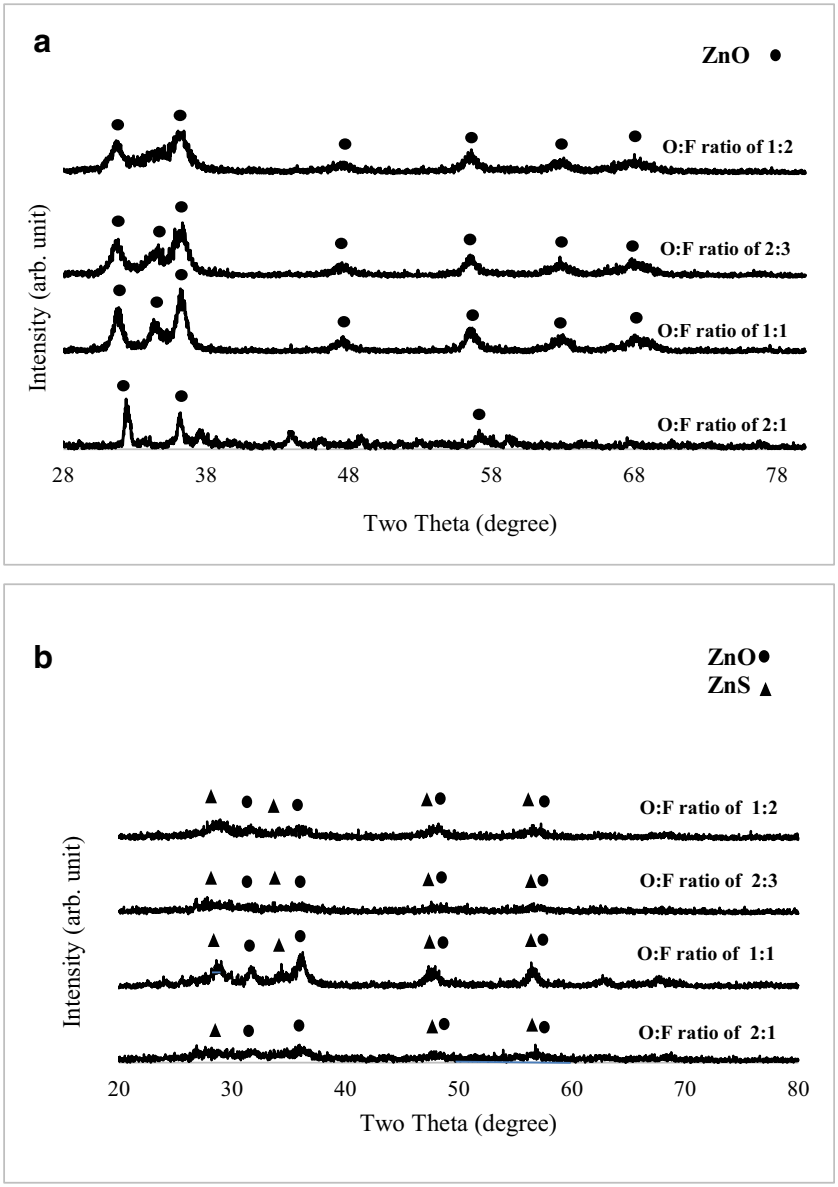

Fig. 1 XRD patterns of (**a**) ZnO and (**b**) ZnO/ZnS powders synthesized using ethylene glycol fuel and different O:F ratios

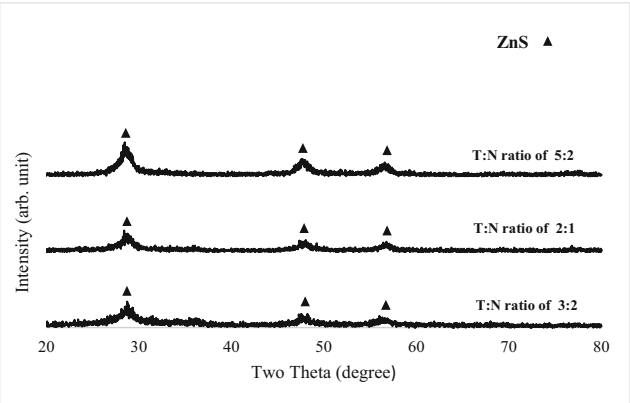

Fig. 2 XRD patterns of ZnS samples synthesized using constant O:F ratio of 2:3 and different ratios of thioacetamide to nitrate (T:N)

Figure 3a, b show XRD patterns of ZnO and ZnO/ZnS composite powders synthesized using ethylene glycol fuel and O:F ratio of 2:3 before and after calcination at 600 °C, respectively. As expected, ZnO nanoparticles calcined at 600 °C for 3 min show sharper and higher peaks due to the higherr crystallinity of the particles. For ZnO/ZnS composite particles, combustion reaction has only led to the formation of ZnS phase. However, after calcination, both ZnO and ZnS phases are observed. It is due to the partial oxidation of ZnS powders during calcination process.

The average crystallite sizes of the samples evaluated by Scherrer Equation are listed in Table 1. As shown, ZnO/ZnS samples have lower crystallite size values. It may be related to suppressing the crystal growth rate of ZnO and ZnS due to the distribution of ignition energy on two fronts, one in ZnO and the other in ZnS. By decreasing the crystallite size in ZnO/ZnS, conditions are provided for the formation of quantum dots.

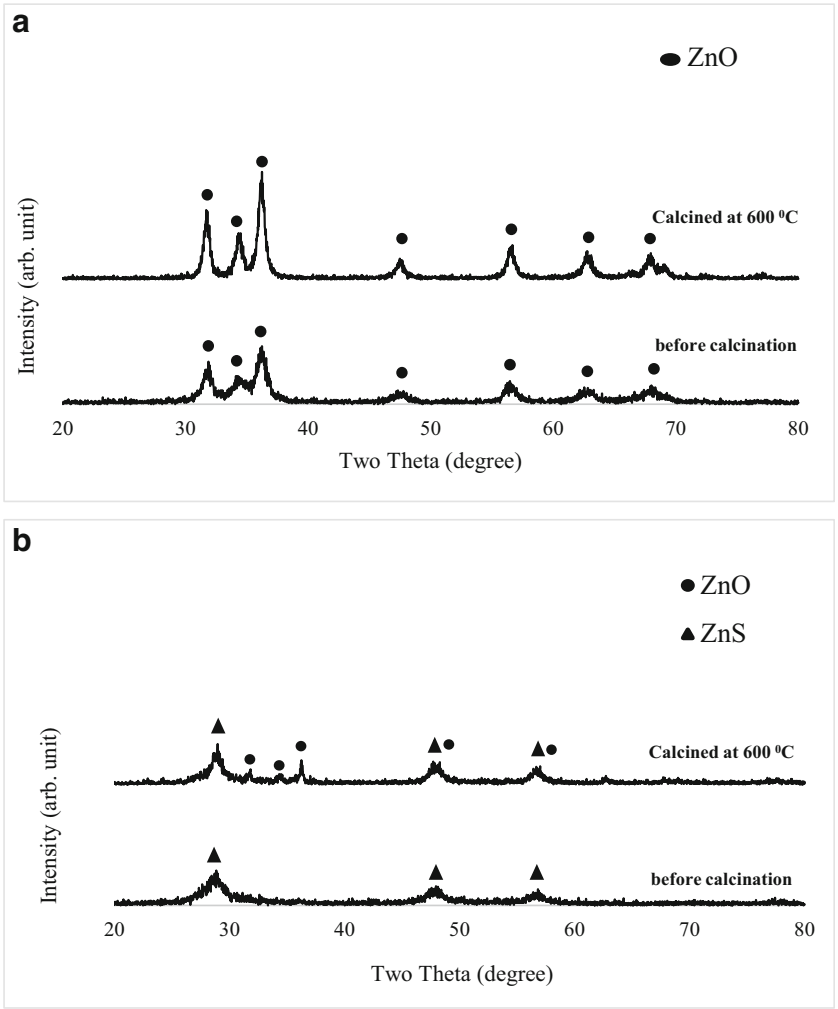

Fig. 3 XRD patterns of (**a**) ZnO and (**b**) ZnO/ZnS composite particles synthesized using ethylene glycol fuel and O:F ratio of 2:3 before and after calcination at 600 °C

Molecular Studies

In all the samples, Zn − O and Zn − S bonds can be easily identified with high intensity peaks in the range of 410–490 cm^{-1} and 600–900 cm^{-1}, respectively [31]. Molecular studies of powders synthesized using ethylene glycol fuel with different O:F ratios were performed with FTIR spectroscopy, mainly for detecting the Zn − O and Zn − S bonds. Some bands observed in most spectra are as follow. Bands at 3000 to 3440 cm^{-1} are related to O − H bonds which have the least intensity in calcined samples due to water evaporation. Also, peak relating to the surface-adsorbed water is located at 1600 cm^{-1} [32,33].The bands at 2900–2930 cm^{-1} are correlated to the CH_3 asymmetric stretching and CH_2 stretching

Table 1 Average crystallite size of ZnO, ZnS and ZnO/ZnS samples determined by Scherrer equation

Sample	O:F ratio	T:N ratio	Crystallite size of ZnO (nm)	Crystallite size of ZnS (nm)
ZnO	2:1	–	19	–
ZnO	1:1	–	11	–
ZnO	2:3	–	9	–
ZnO	1:2	–	7	–
ZnO/ZnS	2:1	1:1	–	–
ZnO/ZnS	1:1	1:1	10	11
ZnS	1:1	3:2	–	7
ZnS	1:1	2:1	–	7
ZnS	1:1	5:2	–	9

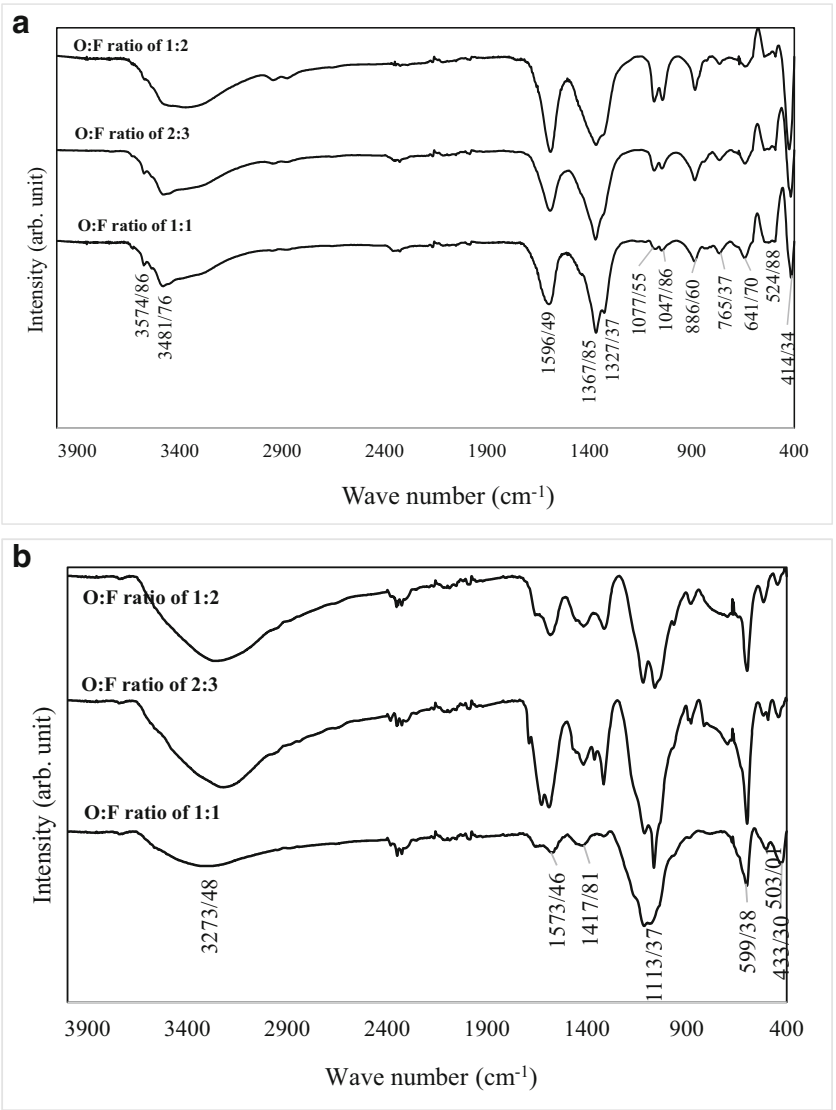

Fig. 4 FTIR spectra of (**a**) ZnO and (**b**) ZnO/ZnS composite particles synthesized with different O:F ratios of ethylene glycol fuels

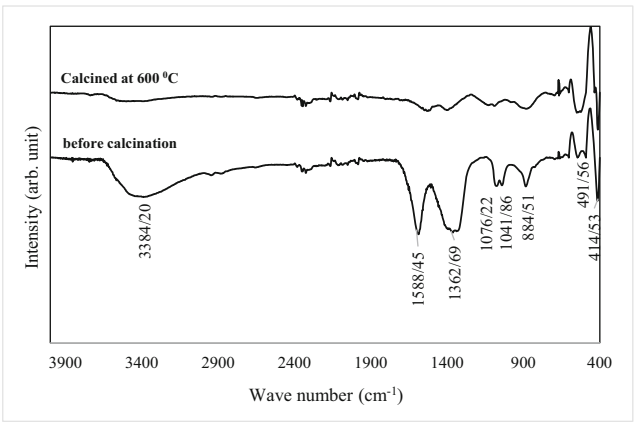

Fig. 5 FTIR spectra of ZnO sample synthesized using ethylene glycol fuel with O:F ratio of 2:3 before and after calcination

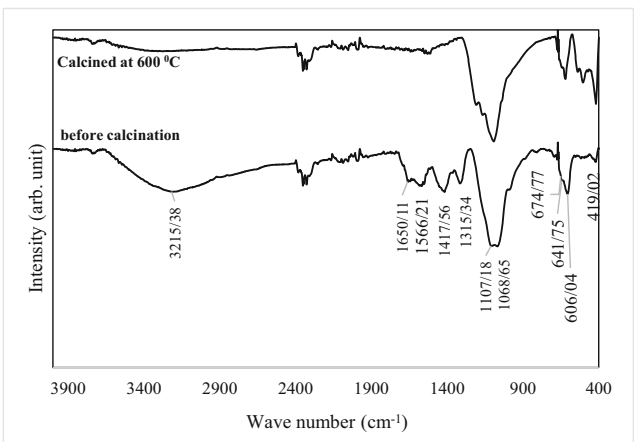

Fig. 6 FTIR spectra of ZnO/ZnS composite sample synthesized using ethylene glycol fuel with O:F ratio of 2:3 and T:N ratio of 2:1 before and after calcination

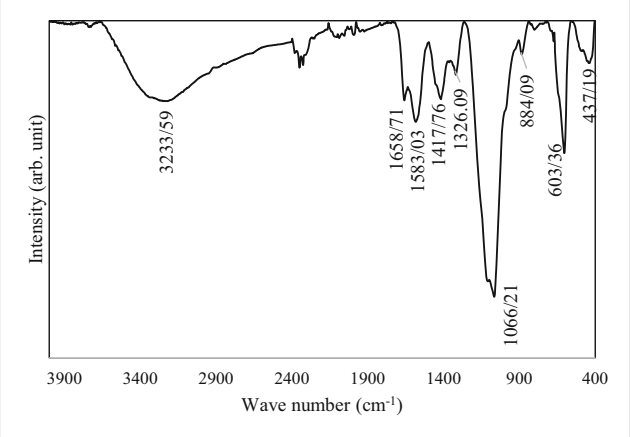

Fig. 7 FTIR spectra of ZnS sample synthesized using ethylene glycol fuel with O:F ratio of 2:3 and T:N ratio of 3:2

[34]. Absorption at 1200 cm^{-1} is due to the stretching vibration of C − O and C − N bonds [35].

Bands at 2110 and 2351 cm^{-1} are related to the absorbance of infrared spectrum by the air molecules [36]. Band at 1400 cm^{-1} is related to N − O bonds from residual nitrate sources after combustion which is sharper for calcined samples. Bands attributing to stretching C=O bond is at 1700 cm^{-1}. In all the samples, Zn − O and Zn − S bonds are easily identified by high intensity peaks in the range of 410–490 cm^{-1} and 600–900 cm^{-1}, respectively [31].

Figure 4a shows FTIR spectra of ZnO samples synthesized using ethylene glycol fuel with different O:F ratios. It can be seen that high intensity peaks in the range of 410–490 cm^{-1} are related to Zn − O bond and the peaks in the range of 500–550 cm^{-1} are attributed to the stretching vibration of Zn − O bond. Other bands are associated to organic compounds mentioned earlier [31].

Figure 4b shows FTIR spectra of ZnO/ZnS composite powders synthesized using ethylene glycol fuel with different O:F ratios. As shown, high intensity peaks in the range of 410–550 cm^{-1} are related to Zn − O bond and the bands in the range of 550–900 cm^{-1} are related to Zn − O and Zn − S bonds. Bands corresponding to Zn − S bond are in the range of 1050–1150 cm^{-1}.The intensity of peaks in the presence of ethylene glycol fuel is higher which may be due to the higher purity and complete combustion reaction. Other bands are associated to organic compounds mentioned earlier [31].

Figure 5 shows FTIR spectra of ZnO sample synthesized using ethylene glycol fuel with O:F ratio of 2:3 before and after calcination. It is obvious that the intensity of carbon and

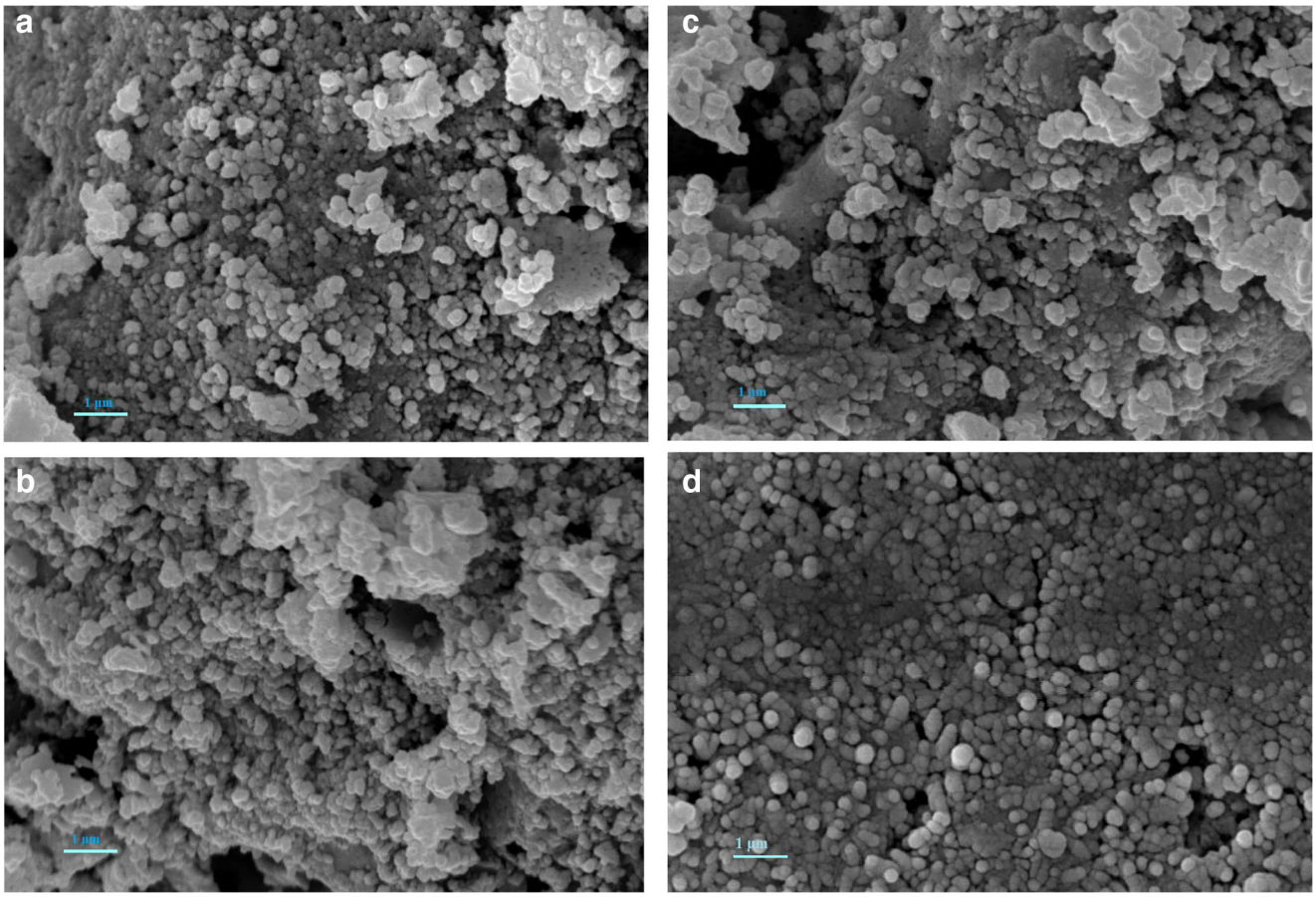

Fig. 8 SEM micrographs of nanoparticles synthesized using ethylene glycol fuel (**a**) ZnO with O:F ratios of 1:1, (**b**) ZnO with O:F ratios of 2:3, c) ZnO/ZnS with T:N ratio of 1:1 and O:F ratios of 1:1 and d) ZnO/ZnS with T:N ratio of 1:1 and O:F ratio of 2:3

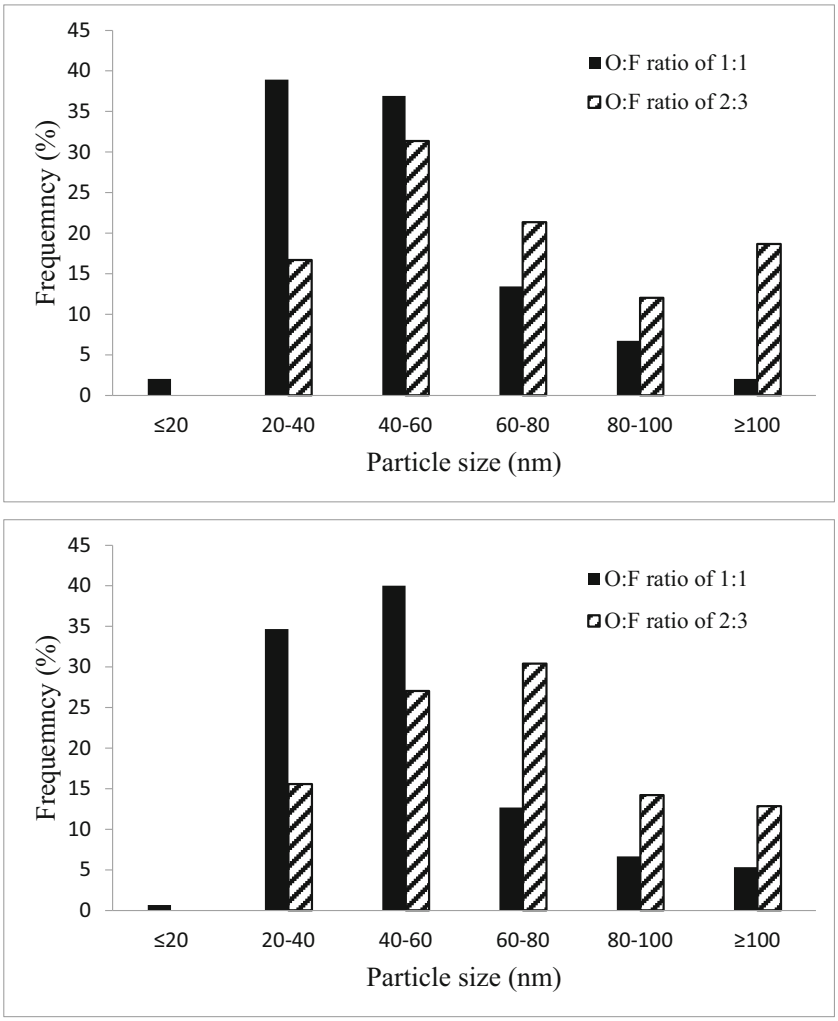

Fig. 9 Particle size distributions of (**a**) ZnO nanoparticles synthesized using ethylene glycol fuel with different O:F ratios of 1:1 and 2:3, and (**b**) ZnO/ZnS nanoparticles synthesized using ethylene glycol fuel T:N ratio of 1:1 and O:F ratios of 1:1 and 2:3

water bands after calcination have decreased, confirming the removal of water and carbon constituents (organic materials). However, the intensity of Zn − O peaks was increased due to the increase of purity and crystallinity after calcination.

Figure 6 shows FTIR spectra of ZnO/ZnS composite sample synthesized using ethylene glycol fuel with O:F ratio of 2:3 and T:N ratio of 2:1 before and after calcination. The intensity of Zn − O bands at 420 cm^{-1} has increased and the peaks corresponding to Zn − S bond in the range of 600–1100 cm^{-1} are sharper and narrower after calcination due to the increase of purity and the burning of carbon. Zn − O bands become more evident after calcination which indicates that the excess organic matters have burnt and powders with higher crystallinity are formed. The bands corresponding to water chemical bonds have lower intensity after calcination which indicates the removal of water during calcination.

Figure 7 shows FTIR spectrum of ZnS powder synthesized using ethylene glycol fuel with O:F ratio of 2:3 and T:N ratio of 3:2. The band at 437 cm^{-1} arises from the low concentration of ZnO in the sample while the sharp and intense peaks in the range of 603–1066 cm^{-1} are related to Zn − S bond which is the dominant phase in this sample. Low combustion intensity and incomplete water vaporization due to the presence of sulfur in the sample are responsible for the appearance of peak at 3200 cm^{-1} for water bond [31].

Microstructure Studies

Figure 8a, b show SEM micrographs of ZnO nanoparticles synthesized using ethylene glycol fuel with O:F ratios of 1:1 and 2:3, respectively. As illustrated, combustion caused to considerable agglomeration of the fine powders. Moreover, the exhaust gases from combustion reaction, such as N_2, NO_2 and CO_2, could increase the porosity of the microstructure [37–41]. The porous microstructure is consisted of fine uniform-distributed spherical nanoparticles. Also, Fig. 8c, d show SEM micrographs of ZnO/ZnS nanopowders prepared using ethylene glycol fuel with different O:F ratios of 1:1 and 2:3, respectively, in the presence of thioacetamide with T:N ratio of 1:1. Combustion heat value of ethylene glycol at 298 K is −1191 ± 10 kJ/mol [42]. Such considerable heat liberated from ethylene glycol may lead to the growth of very fine particles.

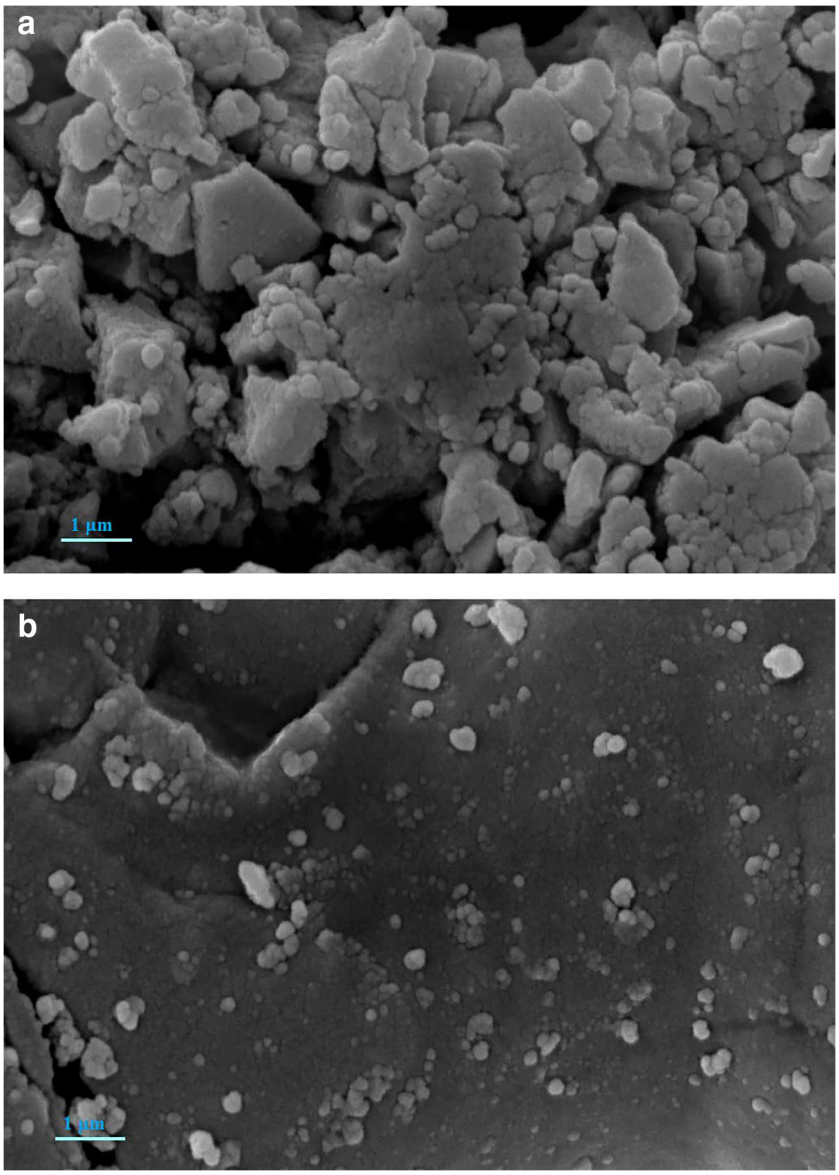

Fig. 10 SEM micrographs of ZnS samples synthesized using different T:N ratios of: (**a**) 2:1, (**b**) 5:2

Based on Fig. 8a, b, particle size distribution of ZnO nanoparticles synthesized using ethylene glycol fuel with different O:F ratios of 1:1 and 2:3 is plotted in Fig. 9a. Similarly, particle size distribution of ZnO/ZnS nanopowders prepared using ethylene glycol fuel with different O:F ratios of 1:1 and 2:3 in the presence of thioacetamide with T:N ratio of 1:1 is shown in Fig. 9b.

As illustrated, stoichiometric ZnO sample (O:F ratio of 1:1) represented narrower particle size distribution than the sample with O:F ratio of 2:3. Similar results were obtained for ZnO/ZnS nanoparticles. According to the results, O:F ratio of 2:3 was selected for the synthesis of ZnO/ZnS nanocompsoites for the subsequent experiments.

Figure 10a, b show SEM micrographs of ZnS samples synthesized using 2:1 and 5:2 T:N ratios, respectively. It seems that the liberated heat of reaction (heat combustion) has decreased at higher T:N ratio, causing less exhaust gases and, consequently, lower porosity and more agglomeration.

XRD patterns (Fig. 3 and Table 1) and SEM micrographs (Fig. 8) of ZnO/ZnS composite nanopowders synthesized using ethylene glycol fuel with O:F ratio of 2:3 confirm that zinc sulfide/zinc composite with least particles in the quantum size range, lower nanocrystallite size and very porous morphology was obtained. It can be seen that the fuel-rich state is more suitable for rapid propagation of ignition and liberation of large amount gases immediately which is ideal to prevent particle size growth [43]. However, the powder in fuel rich state is highly agglomerated. TEM micrograph obtained for this sample is considered for more detailed microstructural analysis (Fig. 11). As illustrated, most of the particles are less than 20 nm or even in quantum dot size range, while they are almost agglomerated due to the nature of the combustion process.

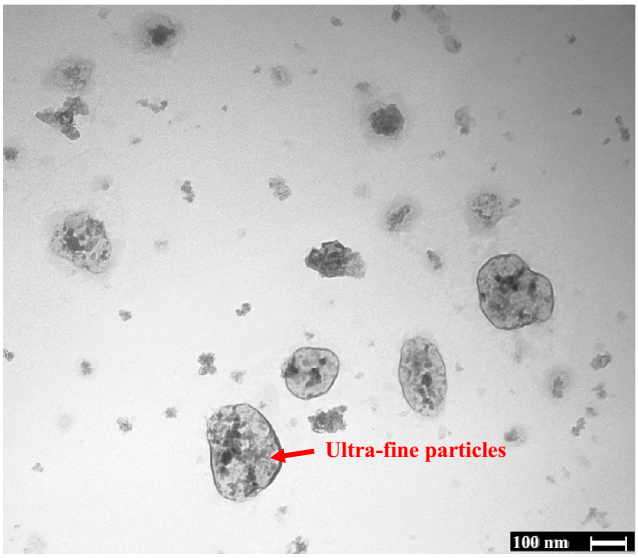

Fig. 11 TEM micrograph of ZnO/ZnS composite nanopowders synthesized using ethylene glycol fuel with O:F ratio of 2:3

Based on the results, four steps are suggested for the competing reactions of ZnO and ZnS (eq.1 and 2) formation: (i) formation of spongy-like ZnO, (ii) nucleation of ZnS quantum dots on the surface of the spongy-like ZnO, (iii) changing of morphology from the spongy-like to semi-sintered flakes during the growth of ZnO/ZnS nuclie, and (iv) the high state of coarsening by Ostwald ripening due to accelerating effect of ultra-fine ZnS particles between ZnO agglomerates.

Photoluminescence Properties

Figure 12a, b show photoluminescence (PL) emission spectra of ZnO and ZnO/ZnS composite particles synthesized using ethylene glycol fuel with different O:F ratios, respectively. As illustrated in Fig. 12a, two peaks at 425 nm and 485 nm are related to high crystalline zinc oxide and lattice defects (such as oxygen vacancy, interstitial oxygen, interstitial zinc, etc), respectively [44–47]. As shown, the most intensity was obtained for the stoichiometric sample due to the complete and strong combustion reaction which led to the formation of more defects and so higher PL intensities than other samples.

As shown in Fig. 12b, ZnO/ ZnS composite particles synthesized using ethylene glycol fuel have two peaks at 425 nm and 485 nm with different intensities. The peak at 425 nm corresponds to zinc oxide/ zinc sulfide structure which has the maximum intensity for stoichiometric sample, indicating the better crystallinity and optical properties of the sample. The peak at 485 nm arises from crystal lattice defects which also has the most intensity for O:F ratio of 1. The least emission intensity was obtained for O:F ratio of 1:2 which has lower optical yield than the sample with O:F ratio of 2:3 due to the higher porosity, finer particles, higher specific surface area and higher combustion reaction intensity. Defects such as oxygen vacancy, zinc vacancy, sulfide vacancy, interstitial oxygen, interstitial zinc, and interstitial sulfide may also enhance the intensity of the emission peaks [44–47]. The peak at 475 nm (blue- green wavelength region) is resulted from the blue shift caused by particle refining. Basically, there aren't any peaks of electronic transitions in pure ZnO in the visible region, but in the combustion process, the high density of surface defects, such as vacancy of oxygen (V_O), changes the visible (especially in blue–green region) to the strongest emission region. Moreover, the transition between ZnS and ZnO and emission due to self- diffusion of Zn in ZnO structure may also occur [48].

Figure 13 shows photoluminescence emission spectra of ZnO powders synthesized using ethylene glycol with O:F ratio of 2:3 before and after calcination at 600 °C. It can be seen that both samples have two intense peaks at 425 nm and 485 nm and a weak peak at 530 nm. Calcination at 600 °C for 5 min increased the emission intensities. It is probably due to the burning of residual carbon constituents, crystal growth, and the decrease of grain boundaries. The combustion of unreacted starting materials can be completed during the calcination, structural defects were increased and consequently, the photoluminescence intensity was increased.

Figure 14 shows photoluminescence emission spectra of ZnO/ZnS composite particles synthesized using ethylene glycol, O:F ratio of 2:3 and T:N ratio of 2 before and after calcination at 600 °C for 5 min. As shown, before calcination, the sample had good green emission in the range of 485–530 nm which was due to the more appropriate reaction using O:F ratio of 2:3than the other ones. On the other hand, addition of thioacetamide could weaken the reaction and introduces more structural defects in the sample including vacancies and interstitials. The weak peak at 425 nm may be also attributed to the increase of thioacetamide and the existence of defects. However, the emission intensities of ZnO/ZnS composite particles were decreased after calcination. It is due to the oxidation of zinc sulfide and the formation of zinc oxide particles with higher crystallinity and less structural defects.

Figure 15 shows photoluminescence emission spectrum of ZnS sample synthesized using ethylene glycol with O:F ratio of 2:3 and T:N ratio of 3:2. The high emission intensity in this sample may be related to the high porosity, finer particles, the increase of specific surface area, and the strong combustion reaction. Similar to previous powders, defects such as oxygen vacancy, zinc vacancy, sulfide vacancy, interstitial oxygen, interstitial zinc, and interstitial sulfide may also enhance the intensity of the emission peaks [44–47]. The peak at 485 nm (blue-green wavelength region) is resulted from the blue shift caused by particle refining. Other evidence of important role of defects on the emission peaks was the high shape similarity of ZnO, ZnO/ZnS and ZnS peaks. For different O:F and T:N ratios, ZnS also showed peaks at different parts of blue-green region due to V_O, self-substitution of Zn_{Zn}, surface imperfects,

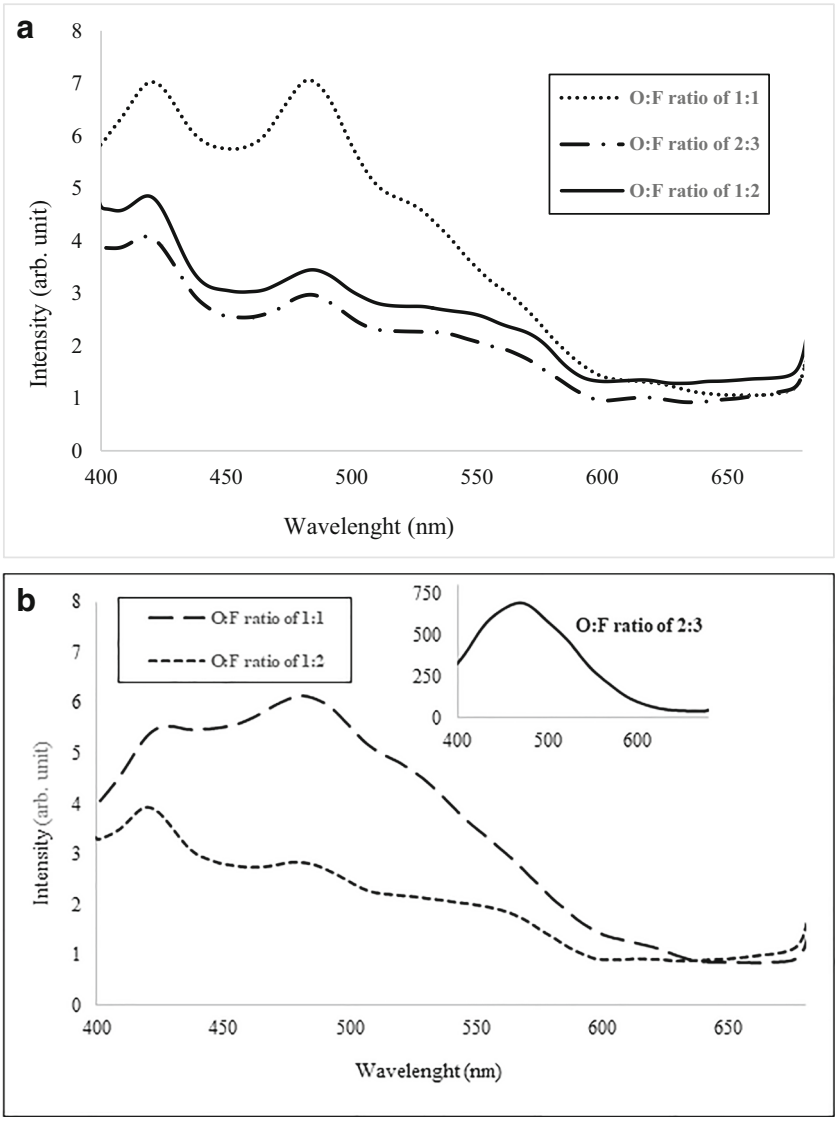

Fig. 12 Photoluminescence emission spectra of (**a**) ZnO and (**b**) ZnO/ZnS composite particles synthesized with different O:F ratios

etc. There weren't seen the role of net structure which can be differed from ZnO to ZnS. The highest level of defects, the best emission condition existed.

The energy level diagram of ZnO, ZnO/ZnS and ZnS samples is shown in Fig. 16. There are three main electron transitions between interstitial Zinc, vacancy of zinc, antisites O_{Zn} and the conduction – valence bands in blue-green region. As shown, the violet emission at 420 nm can be assigned to the electron transition from interstitial zinc to the valance band. The bluish-green emission at 486 nm can be related to the transition of an electron between Zn_i and V_{Zn} levels. The green emission at 526 nm is due to the transition of electron from the conduction band to the antisites O_{Zn}. Sulfur in the structure can act as an activated doped level [49]. Reddy et al. [50] showed that increasing the doping levels in the structure strengthen the green emission. It can be deduced that greenish emission of ZnS samples is due to the formation of ZnS instead of ZnO.

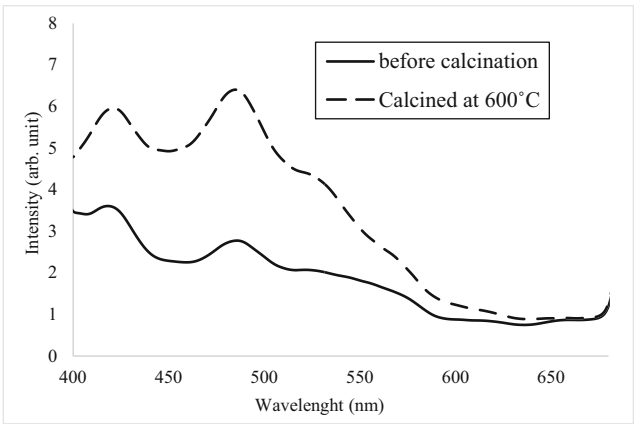

Fig. 13 Photoluminescence emission spectra of ZnO particles synthesized using ethylene glycol with O:F ratio of 2:3 before and after calcination at 600 °C

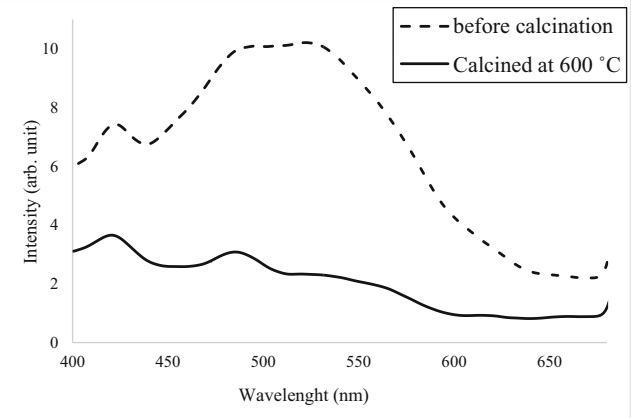

Fig. 14 Photoluminescence emission spectra of ZnO/ ZnS composite particles synthesized using ethylene glycol, O:F ratio of 2:3 and T:N ratio of 2 before and after calcination at 600 °C for 5 min

Band Gap Study

As mentioned before, ZnO/ZnS composite nanopowders synthesized using ethylene glycol fuel with O:F ratio of 2:3 were in the quantum dot size range (Fig. 11) and showed the highest photoluminescence intensity. The estimated band gap of these particles after plotting $(\alpha h\nu)^2$ versus hν and extrapolating the curve in UV region (3–6 eV) (Figs. 16a, b and Fig.17) was 3.4 and 5.4 eV. The former value is close to the band gap of bulk ZnO as reported by many researchers [51–54] and could be lined to the direct transition in r. However, the latter (5.4 eV) may also be calculated and might be due to direct transition in H direction or quantum size effect [55, 56].

Conclusions

Effect of fuel (ethylene glycol) and sulfur source (thioacetamide) concentrations on the solution combustion synthesis of ZnO, ZnO/ZnS and ZnO structure were successfully studied. The results showed that ZnO, ZnS and ZnO/ZnS could be obtained by a one-step combustion process without

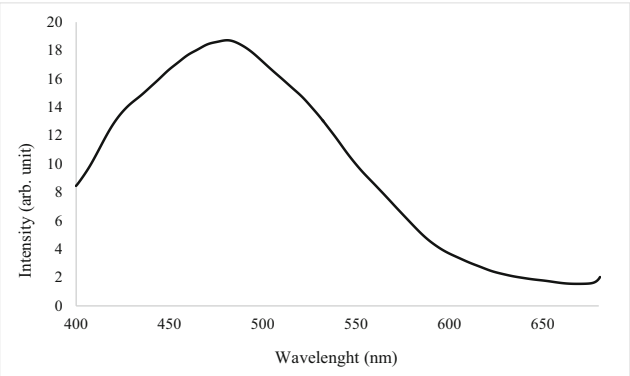

Fig. 15 Photoluminescence emission spectrum of ZnS sample synthesized using ethylene glycol with O:F ratio of 2:3 and T:*N* = 3:2

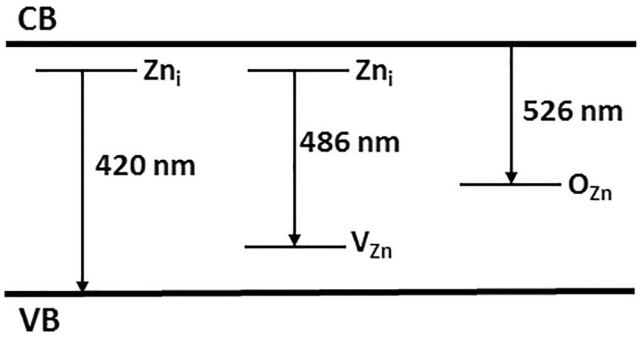

Fig. 16 Energy level diagram in ZnO, ZnO/ZnS and ZnS samples

further calcination need. Nanopowder morphology of agglomerates, Quantum dot size of particles and nanocrystalline nature of primary particles were the results of high-value liberation of large amounts of exhaust gases in a few seconds. The samples showed three main emission peaks in blue – green region at 420, 486 and 520 nm which can be originated from to interstitial zinc, zinc vacancy and antisites O_{Zn}, respectively. Greenish emission was seen in ZnO/ZnS and ZnS due to doping of sulfur in ZnO structure. Although stoichiometric oxidizer to fuel ratio (1:1) had the highest photoluminescence intensity in blue region, but in the case of ZnO/ZnS particles, 2:3 oxidizer to fuel ratio yielded appropriate nanopowders in the range of quantum dot size and the highest photoluminescence intensity in green region.

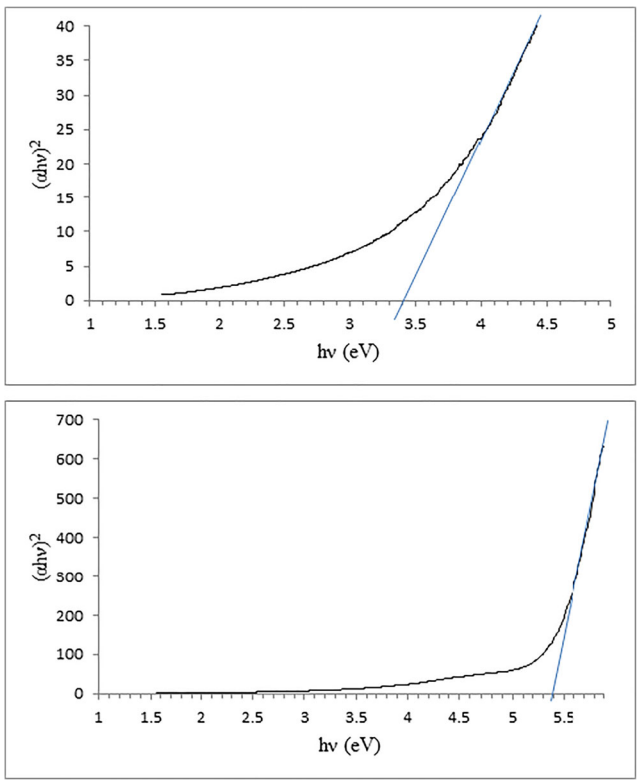

Fig. 17 $(\alpha h\nu)^2$ curve versus hν for ZnS/ZnO composite nanopowders synthesized using ethylene glycol fuel with O:F ratio of 2:3 and T:N ratio of 1:1

References

1. Ben Nasr T, Kamoun N, Guasch C (2008) Physical properties of ZnS thin films prepared by chemical bath deposition. Appl Surf Sci 254:5039–5043
2. M. Sánchez-Agudo, I. Génova, H. Orr, G. Harris and G. Pérez, 2008
3. Chen ZG, Cheng L, Xu HY, Liu JZ, Zou J, Sekiguchi T, Lu GQ, Cheng HM (2010) ZnS Branched Architectures as Optoelectronic Devices and Field Emitters. Adv Mater 22:2376–2380
4. Ruedas-Rama MJ, Orte A, Hall EA, Alvarez-Pez JM, Talavera EM (2011) Quantum dot photoluminescence lifetime-based pH nanosensor. Chem Commun 47:2898–2900
5. Barkhouse DAR, Haight R, Sakai N, Hiroi H, Sugimoto H, Mitzi DB (2012) Cd-free buffer layer materials on Cu2ZnSn(SxSe1−x)4: Band alignments with ZnO, ZnS, and In2S3. Appl Phys Lett 100: 193904
6. Naeimi A, Arabi AM, Shafiee Afarani M, Gardeshzadeh AR (2014) J Mater Sci Mater Electron 25:1575–1582
7. Akbari M, Sharifnia S (2017) Synthesis of ZnS/ZnO nanocomposite through solution combustion method for high rate photocatalytic conversion of CO 2 and CH 4. Mater Lett 194:110–113
8. Naeimi A, Arabi AM, Shafiee Afarani M, Gardeshzadeh AR (2015) J Mater Sci Mater Electron 26:1403–1412
9. Gawai U, Khawal H, Shripathi T, Dole B (2016) A study on the synthesis, pair distribution function and diverse properties of cobalt doped ZnS nanowires. CrystEngComm 18:1439–1445
10. Rasouli S, Arabi A-M, Naeimi A, Hashemi S-M (2018) Microwave-Assisted Combustion Synthesis of ZnO:Eu Nanoparticles: Effect of Fuel Types. J Fluoresc 28:167–172
11. Fang X, Zhai T, Gautam UK, Li L, Wu L, Bando Y, Golberg D (2011) ZnS nanostructures: From synthesis to applications. Prog Mater Sci 56:175–287
12. Esmaeili F, Ghahari M, Shafiee Afarani M, Soleimani A (2018) Synthesis of ZnS–Mn nano-luminescent pigment for ink applications. J Coat Technol Res 15:1325–1332
13. Bredol M, Merikhi J (1998) J Mater Sci 33:471–476
14. Edalati K, Shakiba A, Vahdati-Khaki J, Zebarjad SM (2016) Low-temperature hydrothermal synthesis of ZnO nanorods: Effects of zinc salt concentration, various solvents and alkaline mineralizers. Mater Res Bull 74:374–379
15. Zhao J, Zhang H (2012) Hydrothermal synthesis and characterization of ZnS hierarchical microspheres. Superlattice Microst 51: 663–667
16. Reddy AJ, Kokila M, Nagabhushana H, Chakradhar R, Shivakumara C, Rao J, Nagabhushana B (2011) Structural, optical and EPR studies on ZnO:Cu nanopowders prepared via low temperature solution combustion synthesis. J Alloys Compd 509: 5349–5355
17. Tarwal N, Jadhav P, Vanalakar S, Kalagi S, Pawar R, Shaikh J, Mali S, Dalavi D (2011) P. Shinde and P. Patil. Powder Technol 208:185–188
18. Sharifitabar M, Vahdati Khaki J, Sabzevar MH (2014) Effects of Fe additions on self propagating high temperature synthesis characteristics of TiO2–Al–C system. Int J Refract Met Hard Mater 47:93–101
19. Zarezadeh Mehrizi M, Mostaan H, Beygi R, Rafiei M, Abbasian AR (2018) Reaction Pathways of Nanocomposite Synthesized in-situ from Mechanical Activated Al–C–TiO2 Powder Mixture. Russian Journal of Non-Ferrous Metals 59:117–122
20. Tohidlou E, Ganjkhanlou Y, Kazemzad M, Afarani MS (2010) *Physica Status Solidi C* **7**:2663–2666
21. Ma Q, Wang Z, Jia H, Wang Y (2016) J Mater Sci Mater Electron 27:10282–10288
22. Shahmirzaee M, Afarani MS, Arabi AM, Nejhad AI (2017) In situ crystallization of ZnAl2O4/ZnO nanocomposite on alumina granule for photocatalytic purification of wastewater. Res Chem Intermed 43:321–340
23. Rasouli S, Moeen SJ (2011) Combustion synthesis of Co-doped zinc oxide nanoparticles using mixture of citric acid–glycine fuels. J Alloys Compd 509:1915–1919
24. Aruna ST, Mukasyan AS (2008) Combustion synthesis and nanomaterials. Curr Opinion Solid State Mater Sci 12:44–50
25. Won C, Nersisyan H, Won H, Jeon D, Han J (2010) Combustion synthesis and photoluminescence of ZnS:Mn+2 particles. J Lumin 130:1026–1031
26. M. Shahmirzaee, M. Shafiee Afarani, A. Iran Nejhad and A. M. Arabi, Particulate Science and Technology, 2017, 1–8
27. Lagashetty A, Havanoor V, Basavaraja S, Balaji S, Venkataraman A (2007) Microwave-assisted route for synthesis of nanosized metal oxides. Sci Technol Adv Mater 8:484–493
28. Zahiri M, Afarani MS, Arabi AM (2018) Dual functions of thiourea for solution combustion synthesis of ZnO/ZnS composite powders: fuel and sulphur source. Applied Physics A 124:663
29. Gruy F, Mekki-Berrada MK, Cournil M (2009) AICHE J 55:2553–2562
30. Tauc J, Menth A (1972) J Non-Cryst Solids 8:569–585
31. R. O. Kagel and R. A. Nyquist, Infrared spectra of inorganic compounds (3800–45 cm^{-1}), 1971
32. Hosseini SA, Davodian M, Abbasian AR (2017) Remediation of phenol and phenolic derivatives by catalytic wet peroxide oxidation over Co-Ni layered double nano hydroxides. J Taiwan Inst Chem Eng 75:97–104
33. Hosseini SA, Majidi V, Abbasian AR (2018) Photocatalytic desulfurization of dibenzothiophene by NiCo2O4nanospinel obtained by an oxidative precipitation process modeling and optimization. Journal of Sulfur Chemistry 39:119–129
34. Khosravi H, Eslami-Farsani R (2016) Enhanced mechanical properties of unidirectional basalt fiber/epoxy composites using silane-modified Na+-montmorillonite nanoclay. Polym Test 55:135–142
35. Khosravi H, Eslami-Farsani R (2016) On the mechanical characterizations of unidirectional basalt fiber/epoxy laminated composites with 3-glycidoxypropyltrimethoxysilane functionalized multi-walled carbon nanotubes–enhanced matrix. J Reinf Plast Compos 35:421–434
36. J. G. Omran, M. Sharifitabar and M. S. Afarani, Ceramics international, 2018
37. Chang J, Ahmad MZ, Wlodarski W, Waclawik ER (2013) Self-Assembled 3D ZnO Porous Structures with Exposed Reactive {0001} Facets and Their Enhanced Gas Sensitivity. Sensors 13: 8445–8460
38. F. Xiu, J. Xu, P. C. Joshi, C. A. Bridges and M. Parans Paranthaman, in *Semiconductor Materials for Solar Photovoltaic Cells*, eds. M. P. Paranthaman, W. Wong-Ng and R. N. Bhattacharya, Springer International Publishing, Cham, 2016, https://doi.org/10.1007/978-3-319-20331-7_4, pp. 105–140
39. Das S, Dutta K, Pramanik A (2013) Morphology control of ZnO with citrate: a time and concentration dependent mechanistic insight. CrystEngComm 15:6349–6358
40. Rasouli S, Valefi M, Moeen SJ, Arabi AM (2011) J Ceram Process Res 12:450–455
41. Chae K-W, Zhang Q, Kim JS, Jeong Y-H, Cao G (2010) *Beilstein Journal of Nanotechnology* **1**:128
42. Abdi A, Eslami-Farsani R, Khosravi H (2018) Evaluating the Mechanical Behavior of Basalt Fibers/Epoxy Composites Containing Surface-modified CaCO3 Nanoparticles. Fibers and Polymers 19:635–640
43. Srinatha N, Dinesh Kumar V, Nair KGM, Angadi B (2015) The effect of fuel and fuel-oxidizer combinations on ZnO nanoparticles

synthesized by solution combustion technique. Adv Powder Technol 26:1355–1363
44. Rodnyi P, Khodyuk I (2011) Optical and luminescence properties of zinc oxide (Review). Opt Spectrosc 111:776–785
45. Zeng H, Duan G, Li Y, Yang S, Xu X, Cai W (2010) Blue Luminescence of ZnO Nanoparticles Based on Non-Equilibrium Processes: Defect Origins and Emission Controls. Adv Funct Mater 20:561–572
46. Ji J, Colosimo A, Anwand W, Boatner L, Wagner A, Stepanov P, Trinh T, Liedke M, Krause-Rehberg R, Cowan T (2016) *Scientific reports* **6**:31238
47. Z. O. F. F. P. T. N. Applications, *Claus F. Klingshirn, Andreas Waag, Axel Hoffmann, Jean Geurts*, Springer-Verlag Berlin Heidelberg, 2010
48. Gao X, Wang J, Yu J, Xu H (2015) Novel ZnO–ZnS nanowire arrays with heterostructures and enhanced photocatalytic properties. CrystEngComm 17:6328–6337
49. Vempati S, Mitra J, Dawson P (2012) Nanoscale Research Letters **7**:470
50. Krishna Reddy G, Jagannatha Reddy A, Hari Krishna R, Nagabhushana BM, Gopal GR (2017) Luminescence and spectroscopic investigations on Gd3+doped ZnO nanophosphor. Journal of Asian Ceramic Societies 5:350–356
51. Lin K-F, Cheng H-M, Hsu H-C, Lin L-J, Hsieh W-F (2005) Band gap variation of size-controlled ZnO quantum dots synthesized by sol–gel method. Chem Phys Lett 409:208–211
52. Debanath M, Karmakar S (2013) Study of blueshift of optical band gap in zinc oxide (ZnO) nanoparticles prepared by low-temperature wet chemical method. Mater Lett 111:116–119
53. Köseoğlu Y (2014) A simple microwave-assisted combustion synthesis and structural, optical and magnetic characterization of ZnO nanoplatelets. Ceram Int 40:4673–4679
54. Sakthivel P, Muthukumaran S, Ashokkumar M (2015) J Mater Sci Mater Electron 26:1533–1542
55. Vogel D, Krüger P, Pollmann J (1995) Ab initioelectronic-structure calculations for II-VI semiconductors using self-interaction-corrected pseudopotentials. Phys Rev B 52:R14316
56. Zwicker G, Jacobi K (1985) Experimental band structure of ZnO. Solid State Commun 54:701–704